Supplementary Information

2

S1Updates and parameterization of the radiative transfer model

mSCOPE

- In this supplement, we describe how we adjusted and parameterized the radiative transfer model
- mSCOPE to couple it with the forest model FORMIND.

Support of vertically heterogeneous leaf densities

- FORMIND models the vertical leaf distribution in forest patches explicitly (Henniger et al., 2023a). This
- contrasts with the classical mSCOPE, which builds on the assumption of a vertically homogeneous
- leaf density (Verhoef, 1998). Hence, some adjustments were necessary to accurately incorporate the
- heterogeneous leaf densities resulting from FORMIND into mSCOPE simulations: 11
- The discretization scheme needed to be adjusted. 12
- The probability P_{so} that a leaf is both directly lit by the sun and directly visible to the observer 13 needed to be computed differently to accurately account for hot-spot effects. 14
- Below we first explain corresponding adjustments to the general model setup; then we show how we 15
- discretized the vertical leaf distribution; finally, we discuss necessary model adjustments to capture
- hot-spot effects.

S1.1.1General setup

The mSCOPE model can be formulated as a four-stream ODE system (Yang et al., 2017)

$$\frac{1}{L}\frac{\mathrm{d}E_s}{\mathrm{d}x} = kE_s \tag{S1}$$

$$\frac{1}{L}\frac{\mathrm{d}E^{-}}{\mathrm{d}x} = -sE_s + aE^{-} - \sigma E^{+} \tag{S2}$$

$$\frac{1}{L} \frac{dx}{dx} = -sE_s + aE^- - \sigma E^+
\frac{1}{L} \frac{dE^+}{dx} = s'E_s + \sigma E^- - aE^+
\frac{1}{L} \frac{dE_o}{dx} = wE_s + vE^- + v'E^+ - KE_o,$$
(S2)

$$\frac{1}{L}\frac{dE_o}{dx} = wE_s + vE^- + v'E^+ - KE_o,$$
 (S4)

where E_s is the direct solar flux, E^- the diffuse downward flux, E^+ the diffuse upward flux, and E_o the flux in viewing direction; k, K, s, s', a, σ , v, v', and w are coefficients dependent on the height x; and L is the (constant) leaf density. We may write the system (S1)-(S4) in vector notation as

$$\frac{1}{L}\frac{\mathrm{d}E}{\mathrm{d}x} = f(E),\tag{S5}$$

fluxes change in interactions with leafs.

By making the coefficients dependent on height, the model accounts for vertically heterogeneous leaf properties. The leaf density, however, is assumed to be constant throughout the canopy. This

made it possible to express the integration over the leaf distribution as an integration over space, as

where E denotes the vector of the four fluxes and f is a vector-valued function modelling how the

28 in (S1)-(S4) and (S5):

23

27

$$\frac{\mathrm{d}E}{\mathrm{d}l} = \frac{\mathrm{d}x}{\mathrm{d}l}\frac{\mathrm{d}E}{\mathrm{d}x} = \frac{1}{L}\frac{\mathrm{d}E}{\mathrm{d}x},\tag{S6}$$

where l(x) = Lx is the number of leaf layers below height x. If the leaf density changes with height x,
we need to consider the density gradient $\frac{\mathrm{d}x}{\mathrm{d}l}$. This may be approximated as $\frac{\Delta x(j)}{\Delta l(j)}$, where $\Delta x(j)$ is the
height of leaf layer j and $\Delta l(j)$ the corresponding leaf area index (LAI). Hence, the discretized version
of (S5) can be formulated as follows:

$$E(j+1) = E(j) + f(E(j))\Delta l(j). \tag{S7}$$

That is, the integration scheme of the mSCOPE model still applies, though Δl needs to be adjusted in each height layer.

S1.1.2 Discretization of the forest canopy

To solve system (S1)-(S4), Yang et al. (2017) discretize the canopy into 60 thin leaf layers. They note that the leaf layers must be thin enough so that the LAI per height layer does not exceed approximately 0.1 so as to guarantee numerical stability. In this paper, we used the height discretization of the forest model FORMIND, which splits the forest into vertical layers of 0.5 m height. However, with this approach, LAI values per layer exceeding 0.1 are possible. Hence, we split each FORMIND layer j with $\Delta l(j) > 0.1$ into $\lceil \Delta l(j)/0.1 \rceil$ sublayers prior to applying mSCOPE. Furthermore, we excluded all empty layers, as they do not affect the computed reflectance values and cause numerical issues. As a result, the number of layers depended on the structure of the considered forest.

44 S1.1.3 Hot spot effects

In mSCOPE, the light reaching the observer is computed as a weighted sum of the individual fluxes reaching the observer from each individual height layer:

$$E_o(j_{\text{max}}) = \sum_{j=1}^{j_{\text{max}}} w(j) E_s P_{so}(j) + \left(v(j) E^-(j) + v'(j) E^+(j) \right) P_o(j).$$

Here, $P_o(j)$ is the probability that a light ray emitted at layer j escapes the forest, and $P_{so}(j)$ is

the bi-directional gap probability, i.e., the probability that a light beam from the sun reaches layer j and escapes the forest. Incorporating P_{so} explicitly is necessary to account for hotspot effects, occurring when the sun and the view direction coincide, so that all visible leafs are directly lit by sunlight. While most of the dynamics of the mSCOPE model such as light transmission, scattering 51 and reflection are driven by the leaf density and not directly dependent on the forest height, the 52 probability P_{so} decreases as individual leaf layers are farther apart from one another, making leaf 53 positions less correlated (Verhoef, 1998). Hence, in forests with equal LAI, the hot spot effects will be 54 stronger the denser the leaf layers are packed. Yang et al. (2017) compute P_{so} following the work of Verhoef (1998, pp. 153ff). He computes 56 the probability $P_{so}(j)$ based on probabilities $p_{so}(i,j)$, denoting the likelihood that a light ray reflected 57 in layer j passes through a layer i both from the sun direction and in observer direction. If the two 58 directions are significantly different and the layers i and j are far apart from each other, the horizontal 59 position where the rays in downward and upward direction pass layer j will be far apart from one another. As a consequence, the events of the rays passing through the layer in either direction are almost uncorrelated and independent of layer i where the beam was reflected, i.e., where the rays from the sun and to the observer intersect:

$$p_{so}(i,j) \approx p_s(j)p_o(j).$$
 (S8)

Here, $p_s(j)$ is the probability that a ray from the sun passes layer j, and $p_o(j)$ is the probability that a ray to the observer passes the layer. In contrast, if the two directions coincide or the reflection point is close to the considered layer j, the horizontal locations where layer j is passed in each direction are close together, and the "passing events" are correlated. Verhoef (1998) calls the correlation coefficient between the two events $\rho(i,j)$ and models it as exponentially decaying with (1) the distance d(i,j) at which the two rays pass layer j multiplied by ℓ_0 (2) the inverse of a correlation length constant ℓ , dependent on the leaf size, shape, and inclination:

$$\rho(i,j) = \exp\left(-\frac{d(i,j)}{\ell}\right),\tag{S9}$$

71 where

$$d(i,j) = (x(j) - x(i))\sqrt{\tan^2\theta_s + \tan^2\theta_o - 2\tan\theta_s \tan\theta_o \cos\psi},$$
 (S10)

is computed based on geometrical considerations (c.f. Fig. 8.1 in Verhoef, 1998) with x(j) being the height of layer j above the ground. As computing ℓ from other parameters is complex, Verhoef (1998) assumes it is a given constant. Using the definition of the correlation coefficient, he obtains

$$p_{so}(i,j) = p_s(j)p_o(j) + \rho(i,j)\sqrt{p_s(j)p_o(j)(1-p_s(j))(1-p_o(j))}$$
(S11)

$$= p_s(j)p_o(j) + \exp\left(-\frac{d(i,j)}{\ell}\right)\sqrt{p_s(j)p_o(j)(1-p_s(j))(1-p_o(j))}.$$
 (S12)

If the leaf density is constant, $p_s(j)$ and $p_o(j)$ are independent of the layer j, and both p_{so} and P_{so} can be derived in closed form via integrals over continuous space (Verhoef, 1998, pp. 154f) or, equivalently, the cumulative leaf density. If the leaf density is different in each layer, however, we may fall back to the discrete model version and compute the probability P_{so} as

$$P_{so}(j) = \prod_{k=j}^{j_{\text{max}}} p_{so}(i,k).$$

As $P_{so}(j)$ needs to be computed for each layer, this algorithm runs in $\mathcal{O}(n^2)$, where n is the number of considered layers. This can be inefficient. However, if the correlation $\rho(i,k)$ is small for $k>j_0$ for some j_0 , it is $p_{so}(i,k)\approx p_s(k)p_o(k)$, and we can write

$$P_{so}(j) \approx \left(\prod_{k=j}^{j_0} p_{so}(i,k)\right) \left(\prod_{k=j_0+1}^{j_{\text{max}}} p_s(k) p_o(k)\right). \tag{S13}$$

$$= P_s(j_0 + 1)P_o(j_0 + 1)\prod_{k=i}^{j_0} p_{so}(i, k),$$
(S14)

where $P_s(j_0+1)$ is the probability that a light ray from the sun reaches layer j_0+1 undisturbed, and $P_o(j_0+1)$ is the probability that a light ray from layer j_0+1 reaches the observer undisturbed. Equation (S14) can be computed for all layers in $\mathcal{O}(n)$, since the number j_0-j of layers with a significant correlation is bounded by a constant. We defined j_0 as the first layer j where $\rho(i,j) < 10^{-5}$. Following Yang et al. (2017), we computed the correlation length ℓ as

$$\ell = \frac{2w_l}{k + K},\tag{S15}$$

where w_l is the (species-dependent) width of a leaf, which we assumed to be 5 cm independent of the height of the considered layer.

89 S1.2 Reduced sunfleck observation on soil

86

100

The probability $P_{so}(0)$ that a location on the ground is both directly lit by sunlight (sunfleck) and visible to the observer is generally computed according to Eq. (S14). Depending on the parameterization and the forest density, sunflecs can account for a major share of the computed reflectance, especially for short wavelengths. However, the structure and cover of the ground (grass / herb cover, deadwood, etc.) are typically unknown and may significantly reduce the visible ground portion. To account for this issue and reduce the potential for bias, we set $P_{so}(0) = 0$ in this study. This model adjustment does not invalidate the modelled energy fluxes, as reflection of light into the diffuse upward stream is still considered. Instead, we made the additional assumption that no sunlit ground is directly visible to the observer.

We based our parameterization of mSCOPE on the work of Henniger et al. (2023a) but adjusted the

99 S1.3 Parameterization of the radiative transfer model

leaf parameters based on values from the TRY data base (Kattge et al., 2011) where available. We 101 submitted a TRY data request on July 30th 2024 regarding data on the leaf chlorophyll content per leaf 102 area and the leaf carotenoid content per leaf area. We refined the resulting data to include only species of the considered genera and filtered the data by the respectively most frequent unit, namely g/m² 104 for the chlorophyll content and $\mu g/cm^2$ for the carotenoid content. The selected data were originally 105 published by Medlyn et al. (1999) and Lukeš et al. (2013) for the chlorophyll content and Lukeš et al. 106 (2013) for the carotenoid content. 107 We computed the mean of the chlorophyll and carotenoid content for each genus. No chlorophyll 108 content estimates were available for Populus, so we kept the original value used in Henniger et al. (2023a). For the carotenoid content, estimates were only available for Pinus, Picea, and Betula. We 110 kept the other values by Henniger et al. (2023a) but noted that the updated carotenoid values for 111 Pinus and Picea were significantly higher than the originals. Furthermore, we noted that the updated 112 carotenoid / chlorophyll ratio of all genera except Fagus and Quercus was about 1/4. Hence, we 113 adjusted the carotenoid content for theses genera based on the latter carotenoid / chlorophyll ratio to

	Pinus	Picea	Fagus	Quercus	Populus	Betula	Robinia
Chlorophyll a+b content $\left[\frac{\mu g}{cm^2}\right]$	56	37	41	31	44	29	36.71
Leaf mass per unit area $\left[\frac{g}{cm^2}\right]$	0.024	0.025	0.014	0.014	0.007	0.006	0.006
Equivalent water thickness [cm]	0.003	0.003	0.017	0.017	0.009	0.0102	0.0102
Senescence material (brown pigments) [-]	0.01	0.01	0.01	0.01	0.01	0.01	0.01
Carotenoid content $\left[\frac{\mu g}{cm^2}\right]$	12.5	7.5	10	8	9.38	6.9	8.62
Leaf structure parameter [-]	1.25	1.24	2.6	2.6	1.30	1.77	1.77

Table S1: Adjusted parameters for the considered genera.

avoid issues arising from inconsistent data adjustment. The resulting optical leaf parameters we used are displayed in Table S1.

117 S2 Description of the Monte Carlo approach to generate forest stands ("Forest Factory")

119 S2.1 Background and previous work

132

In this paper, we generated forest stands via a Markow Chain Monte Carlo (MCMC) approach. Our 120 method is based on the "Forest Factory", introduced by Bohn and Huth (2017) and further improved 121 by Henniger et al. (2023b). The goal of the Forest Factory is to construct large numbers of forest 122 stands with different structure and species composition by randomly adding trees to a forest as long 123 as it is in an ecologically feasible state. A stand is considered feasible if the GPP of each tree suffices 124 to satisfy its respiratory needs. Hence, the state space of possible forests consists of all those stands 125 where each tree is sufficiently productive. The state space can be filtered by further constraints, such 126 as available space. 127 The original idea of the Forest Factory was to conduct a hierarchical sampling approach to randomly 128 generate possible forest states: first, a minimal and a maximal tree height h_{\min} , h_{\max} is drawn from 129 some stochastic distribution; second, a set of species that can attain heights in $[h_{\min}, h_{\max}]$ is randomly 130 assembled; and third, a maximal crown volume V is randomly drawn. Then, the forest stand is filled 131

with trees by first drawing tree heights in $[h_{\min}, h_{\max}]$ and then corresponding species from the species

pool until the forest stand is "full", i.e., the crown volume V has been reached or another constraint is

134 not fulfilled (space or productivity constraint).

If only the productivity constraint is violated, i.e., despite enough space in the forest, there are trees whose maintenance respiration exceeds their GPP, an attempt is made to bring the forest stand into a feasible state by changing the species of the trees in question. If trees with insufficient GPP can be replaced by trees with different species but the same heights, more trees are added to the forest until no addition is possible. That way, the chances of reaching the target crown volume V increase. In summary, the Forest Factory attempts to generate forests that match the pre-sampled forest characteristics as well as possible.

In this study, we took a slightly different approach motivated by the following considerations. First, 142 the original approach can yield forest states in which some trees are not able to fulfill their respiratory 143 needs. This is because any species adjustment made to satisfy the productivity constraint also affects 144 the productivity of other trees, potentially making them violate the productivity constraint, in turn. 145 In favour of computational efficiency, Henniger et al. (2023b) did not consider such secondary effects in 146 already processed trees, potentially leading to infeasible states. Second, every adjustment to the forest 147 state would require updating the productivity of all trees considering water and light competition, 148 which, in turn, is computationally costly. Therefore, the original Forest Factory took a simplified 149 approach not taking the entire year's climate into account when updating the productivity of trees. 150 Third, the optimization approach attempting to find more suitable species for trees whose GPP fell 151 below their maintenance respiration leads to a bias towards species with higher carbon use efficiency. 152 Fourth, the approach makes it difficult to interpret the results in a statistically rigorous manner. 153

154 S2.2 Revised algorithm of the Forest Factory

We updated the Forest Factory approach by dropping the step of pre-sampling the crown volume (first 155 drawing a "target crown volume", then assembling a forest with this crown volume) and considering 156 the crown volume as an emerging property, i.e., sampling from forest states with the given height 157 range and species pool. Similar to Henniger et al. (2023b), we started by drawing a height range and 158 a species pool. Then we added and removed trees randomly, so that the forest emerging after many addition / removal steps could attain both small and large crown volumes. As we did not attempt 160 to reach a specific target crown volume, no optimization step adjusting tree species was necessary. 161 Instead, we accepted all steps where none of the constraints was violated and rejected all other steps, 162 falling back to the respective previous state. After a limited number of iterations, we terminated the 163 process. Below we provide further details.

S2.2.1Feasibility 165

166

174

We sought to simulate forests that satisfy the following constraints: (1) the GPP of each tree should be at least as high as its required maintenance respiration ("productivity constraint), and (2) the forest's 167 crown area should not exceed the forest area in any height level ("space requirement constraint"). If a 168 forest state satisfies all criteria, we call it "feasible". 169 To evaluate whether a forest stand was feasible, we first checked the space constraint, es it is easy 170 to verify based on the crown dimensions of the trees and does not require simulation of carbon fluxes. 171 If the space constraint was satisfied, we computed the total GPP and maintenance respiration for all 172 trees in the stand for one year, taking into account water and light competition as well as temperature 173

effects. Then we checked for each tree whether its GPP satisfied its respiratory needs.

S2.2.2Pre-sampling 175

Before generating a forest stand, we randomly drew a minimal and a maximal height h_{\min} , h_{\max} 176 uniformly from the interval [5.8 m, 50 m]. Then we determined the set $S_{h_{\min}}$ of species that can attain 177 heights of at least h_{\min} . Next, we drew a number N from the discrete uniform distribution over the 178 set $\{1,\ldots,|S_{h_{\min}}|\}$, where $|\cdot|$ denotes the number of elements. Finally, we drew N species from $S_{h_{\min}}$ 179 under the condition that at least one of the selected species can reach height h_{max} . The resulting set \bar{S} contained the species pool for the next generated forest. These pre-sampling steps followed the 181 approach by Henniger et al. (2023b). 182

S2.2.3Steps 183

Starting from an initial forest (see below), we iteratively changed the forest state by adding or removing 184 trees. Let X_i denote the forest state after i attempts to change it. We generated the next forest state 185 X_{i+1} as follows: with probability 0.5, we either randomly added or removed a tree to / from X_i (details 186 below), arriving at a new forest state X'_i . Then we checked if the proposed state X'_i was feasible. If it 187 was, we accepted the proposed state, setting $X_{i+1} := X'_i$, making it the new forest state. Otherwise, 188 we rejected the change, $X_{i+1} := X_i$, leaving the forest state unchanged. 189 As the feasibility check is computationally costly, we used an adaptive step size k between consecutive feasibility checks. That is, we performed k tree additions or removals and rejected all changes 191 jointly if the resulting proposed state was infeasible. We started with a step size of k=5 and adjusted 192 the step size dynamically during the simulation based on the success of previous feasibility checks. 193 When 5 consecutive feasibility checks were successful, we doubled k; when 5 consecutive feasibility 194 checks were unsuccessful, we divided it by 2 (rounding down to the next integer). However, we never 195

allowed step sizes below 1 and refrained from further step size increases if $k \geq 10$.

197 S2.2.4 Initialization

To reduce the required burn-in time until the simulation reaches its limiting distribution, we did not start with an empty forest ("bare ground") but from a "half-full" forest. To that end, we randomly added trees to the forest (see next section for details on how the trees' properties were selected) until their crown occupied half of the volume that a forest of height of h_{max} could attain, i.e., $h_{\text{max}} \cdot A$, where A = 0.04 ha is the ground surface area of the forest stand. Then we evaluated the feasibility of the forest stand. If the forest stand was infeasible, we randomly removed half of the trees and checked the feasibility again. If the state was still not feasible we repeated this procedure until a feasible state was found. Note that an empty forest (no trees) always satisfies the feasibility constraints.

206 S2.2.5 Adding / removing a tree

When adding a tree, we randomly drew its height h from a conditional exponential distribution with rate parameter $\lambda=0.05$, conditioned to the interval $[h_{\min},h_{\max}]$ using the inversion method (Henniger et al., 2023b). Next, we determined the set $S_h \subseteq S_{h_{\max}}$ of all species that could attain a height of h. Finally, we randomly drew the tree's species from the set S_h . In Formind, tree height and species suffice to fully characterize a tree, and all other static properties (e.g. DBH, crown diameter, etc.) can be computed from this information via allometric relationships.

When removing a tree, we randomly selected any of the forest stand's trees and removed it. In
cases where the forest was empty and no trees could be removed, we switched to adding a tree instead.

$\mathbf{S2.2.6}$ Termination

We terminated the procedure after a number of at least 200 individual tree additions and removals
had been reached. In the hypothetical case that the final forest did not contain any tree, we continued
attempting to add a tree until at least one tree was present. Note that only in exceptional cases with
very harsh climatic conditions, forest states with a single tree could be infeasible.

$_{\scriptscriptstyle 20}$ S3 Distributions of key characteristics of the generated forests

In this study, we generated large numbers of 0.04 ha forest stands via a Markow-Chain-Monte-Carlotype approach. These forests differed greatly in their species composition and heterogeneity. The
distributions of key forest characteristics among the data set are displayed in Fig. S1. Besides the
forest attributes used in this study, we also plotted the distribution of the basal-area-weighted Shannon

entropy in the forest stands. In contrast to the classical Shannon entropy, this diversity measure also incorporates the size (basal area) of the individuals rather than only their number. That is, the entropy is maximized, when all present species have the same basal area rather than the same abundance.

228 S4 Computation of the basal-area-weighted DBH entropy

In the main text, we used the basal-area-weighted DBH entropy $S_{\rm DBH}$ (Fischer et al., 2024) as a measure for structural diversity. Specifically, this quantity measures the diversity of DBH values in a forest stand taking into account that the ecological effect of large trees is much higher than that of small trees. The basal-area-weighted DBH entropy is computed as follows:

$$S_{\text{DBH}} = -\int_{0}^{\infty} f_{\text{d}}(\delta) \ln f_{\text{d}}(\delta) d\delta, \tag{S16}$$

where $f_{\rm d}(\delta)$ is the estimated probability density of finding trees with DBH δ in the stand, weighted by basal areas. Following Fischer et al. (2024), we estimated $f_{\rm d}(\delta)$ using a kernel-density estimation (see e.g. Wand and Jones, 1995):

$$f_{\rm d}(\delta) = \sum_{d \in D} w_d K(d, \delta; h). \tag{S17}$$

Here, D contains the DBH values of all trees in the forest patch (including repetitions if applicable), and

$$K(d, \delta; h) = \begin{cases} \frac{3}{4h} \left(1 - \left(\frac{d - \delta}{h} \right)^2 \right) & \text{if } |d - \delta| \le h \\ 0 & \text{else} \end{cases}$$

is the Epanechnikov kernel with bandwidth $h=1\,\mathrm{cm}$, which measures how similar two DBH values are considered. DBH values d and δ with $|d-\delta|\geq h$ are considered completely dissimilar. The weights

$$w_d = \frac{d^2}{\sum_{d \in D} d^2} \tag{S18}$$

express the individual trees weights according to their respective basal areas.

For a more in-depth discussion of the basal-area-weighted DBH entropy refer to Fischer et al. (2024) and its supplement.

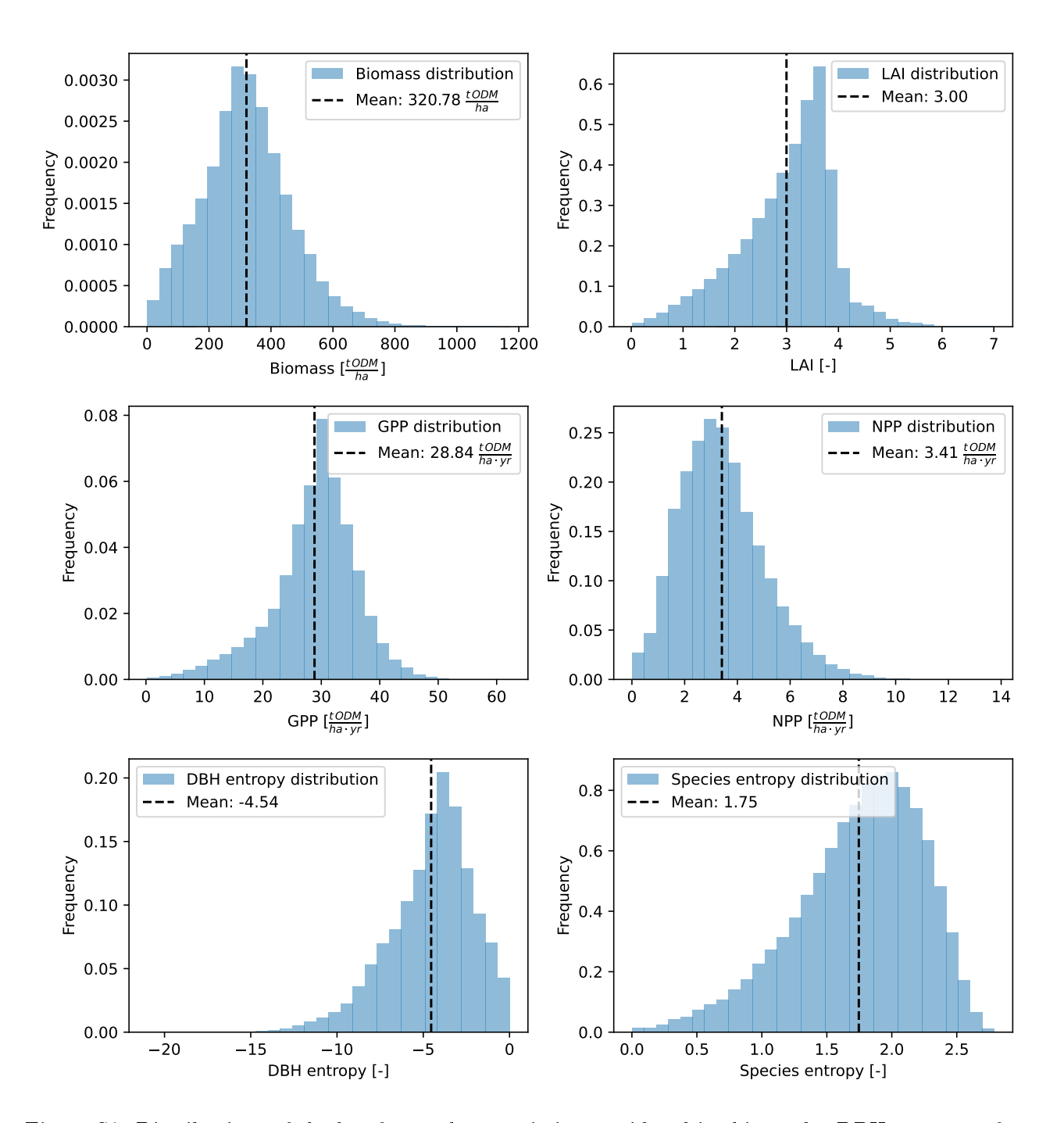


Figure S1: Distributions of the key forest characteristics considered in this study. DBH entropy refers to the basal-area weighted DBH entropy (Fischer et al., 2024). The species entropy denotes the basal-area-weighted Shannon entropy in the forest stands.

43 S5 Updates to the parameterization of FORMIND for temperate forests

In this supplement, we provide the temperate forest parameterization of the forest model FORMIND that we used to simulate a large dataset of forest stands. We derived the parameterization from 245 the work of Bohn et al. (2014), but adjusted it to (1) better reflect forest dynamics in structurally 246 heterogeneous forests and (2) match the environmental conditions found at the Hohes Holz site used 247 for the parameterization. To parameterize the model, we used allometric data from the Tallo database 248 (Jucker et al., 2022), forest inventory data from the Hohes Holz site (10 ha), soil-type-specific values for hydrological parameters (Maidment, 1993), and unpublished soil and LAI data obtained on site. The Hohes Holz site is a mixed deciduous / evergreen ICOS forest site located in central northern 251 Germany (mean ann. temperature 10.4°C; mean ann. precipitation 5171/m²; Holtmann et al., 2021). 252 We sought to minimize changes of the original parameterization where possible. Hence we focus on 253 presenting the changes to the original parameterization and do not provide further details on FORMIND 254 or the work by Bohn et al. (2014). We begin by providing an overview of the parameterization approach and the changes we introduced, then we provide details on individual steps where necessary. Finally, 256 we provide a brief analysis of the dynamics of the updated model. 257

258 S5.1 Overview

262

263

264

265

266

268

269

270

272

259 S5.1.1 General approach

When updating the FORMIND parameterization for temperate forests (here: Hohes Holz site), we sought to satisfy the following criteria:

- 1. Agreement with field data.
 - The allometric equations and the representation of environmental conditions should match observations from inventory and eddy flux field data.
 - The mean LAI computed based on the forest inventory should match the independent on-site LAI estimate from the Hohes Holz site.
 - Productivity and respiration should be parameterized so that for most of the trees in the inventory, the gross primary production (GPP) exceeds the respiratory needs for maintenance (see Fischer et al., 2024).
 - 2. Consistency with first principles.
 - The maintenance respiration of trees should increase monotonously with the tree size.
 - Temporal upscaling of reference environmental conditions should be conducted consistently.

- 3. Consistency with expectations on long-term dynamics.
 - The forest succession should yield a "reasonable" forest trajectory.

Besides satisfying these criteria, we also enabled model features that were developed after the initial work by Bohn et al. (2014) and improve the model's mechanistic realism. Nonetheless, we pursued to limit the changes of the parameterization to the necessary minimum so as to facilitate consistency with previous work.

279 S5.1.2 Overview of changes

273

274

The allometric relationships for tree height, biomass, and crown diameter were fitted based on data from the Tallo database (Jucker et al., 2022). Then the LAI was adjusted, ensuring that (1) the mean LAI of the Hohes Holz forest matched an independent estimate and (2) the maintenance respiration is monotonously increasing with tree size. The balance between trees' maintenance respiration and other carbon losses (e.g. growth respiration) was fitted by constraining the maintenance respiration based on the estimated productivity of trees in the Hohes Holz forest stand. Finally, the mortality was adjusted based on simulations of the forest succession.

We enabled the defoliation mechanism (first introduced by Fischer et al., 2024) as a consistent way to account for trees whose respiratory needs exceed their gross primary productivity (GPP). To keep the overall mortality consistent with field data, we reduced the stochastic background mortality. Furthermore, we enabled a regeneration mechanism based on the available light. Lastly, we adjusted the soil and weather parameters based on the conditions found at the Hohes Holz site, and we adjusted the climatic reference conditions that FORMIND uses to infer maintenance respiration based on the updated parameterization.

294 S5.2 Details

Below we provide further details regarding individual parameterization steps. The order of the sections reflects the execution order of the steps, as some parameterization results depend on one another.

297 S5.2.1 DBH-height relationships

To fit the DBH-height relationships, we used allometry data from the Tallo database (Jucker et al., 2002). This dataset contains more than 5,000 observations for Picea and Fagus, about 1,000 for Fraxinus and Betula, 643 and 445 for Quercus and Populus, respectively, and 18 for Robinia.

We assumed that the height is log-normally distributed around the mean, which is used in the model. This allowed us to fit the DBH-height relationship via an ordinary least squares fit on log-

	Pinus	Picea	Fagus	Quercus	Populus	Fraxinus	Betula	Robinia
h_0 [m]	81.1	61.46	124.08	57.05	48.51	57.23	56.63	66.91
h_1 [m ^{h_2}]	0.93	0.39	1.8	0.46	10^{5}	0.35	10^{5}	10^{5}
h_2 $[-]$	0.85	1.15	0.67	1.	0.62	1.	0.66	0.7

Table S2: Adjusted parameters for the DBH-height relationships.

transformed data. We tested different functional relationships between DBH and height:

$$h(d) = h_0 d^{h_1}, (S19)$$

$$h(d) = \frac{h_0 d}{h_1 + d}. ag{S20}$$

We found that each of the functional forms is optimal for some of the considered genera. Hence, we introduced a new, generalized relationship:

$$h(d) = \frac{\tilde{h}_0 d^{\tilde{h}_2}}{\tilde{h}_1 + d^{\tilde{h}_2}}.$$
 (S21)

We applied the AIC criterion (Akaike, 1974) to determine whether to use one of the simpler models 306 (S19) or (S20), or the joint model. Where model (S19) was optimal, we used the joint (S21) model with parameters $\tilde{h}_0 = 10^5 h_0$, $\tilde{h}_1 = 10^5$, and $\tilde{h}_2 = h_1$ after fitting the parameters of model (S19). This is an 308 approximation to the limit of $\tilde{h}_0, \tilde{h}_1 \to \infty, \frac{\tilde{h}_0}{\tilde{h}_1} \to h_0$, where model (S21) reduces to model (S19). Only 309 for populus, we manually chose model (S19) instead of model (S21), because (a) the latter would have 310 implied that trees need an excessively large DBH to reach their maximal height and (b) the difference 311 in AIC between the models was small, justifying the choice of the simpler model (Δ AIC < 10). 312 We chose model (S19) for the following genera: Populus, Betula, and Robinia. We chose model 313 (S20) for Quercus and Fraxinus, and model (S21) for Pinus, Picea, and Fagus. The resulting parameters 314 are displayed in Table S2, and the resulting curves, compared to the original DBH-height-relationships, 315 are displayed in Fig. S2. 316

317 S5.2.2 DBH-biomass relationships

The stem biomass can be computed from the DBH based on rather simple geometrical assumptions and therefore with relatively high credibility. It is therefore a sensible tool to check the consistency of direct biomass estimates that were derived based on data not covering the entire range of possible trees

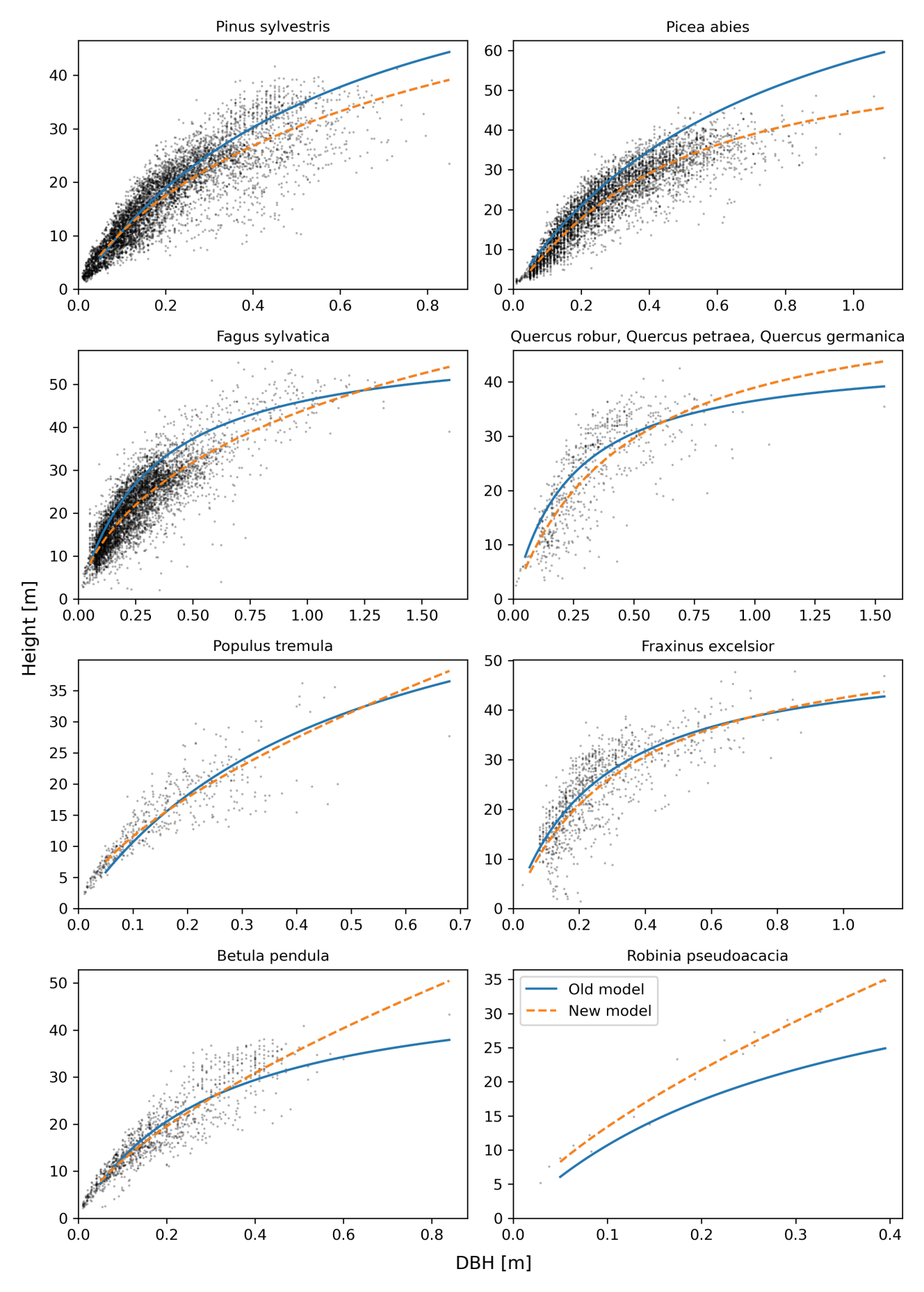


Figure S2: DBH-height relationships for the considered species / genera. The black dots display the data from the Tallo database (Jucker et al., 2022); the solid blue curves show the relationships as they were in the old parameterization, whereas the dashed orange lines show the newly fitted curves.

	Pinus	Picea	Fagus	Quercus	Populus	Fraxinus	Betula	Robinia
b ₀ [-]	1.202	1.213	1.180	1.232	1.363	1.237	1.227	1.389
b_1 [-]	7222.6	78.61	15395	7802	5542	34929	5391.9	7213.9
b_2 $[-]$	3.675	3.679	3.474	3.575	3.795	3.530	3.631	3.497

Table S3: Adjusted parameters for the DBH-biomass relationships.

sizes. Moreover, in the updated parameterization, the crown biomass (= total biomass-stem biomass) 321 is also used to estimate how much crown damage a tree can tolerate before dying. Therefore, we sought 322 DBH-biomass relationships where stem biomass and total biomass were consistent with one another. 323 To enforce such a consistent parameterization of stem biomass and tree biomass, we assumed that 324 the stem biomass is always at least 90% of the tree biomass. That is,

$$B(d) = \max\left(B_0(d), \frac{1}{0.9}B_s(d)\right),$$
 (S22)

where B is the total tree biomass,

339

$$B_0(d) = \exp\left(\frac{b_0 \left(\ln(d \cdot C) - b_2\right) \left(2b_1 + \ln(d \cdot C) - b_2\right)}{b_1 + \ln(d \cdot C) - b_2}\right) \text{ [t ODM]}$$
(S23)

with conversion factor $C=100\frac{1}{m}$ is the tree biomass equation derived by Bohn et al. (2014) based on 327 data by Schober (1995), and B_s is the stem biomass computed based on tree geometry and allometric 328 equations. 329 The resulting curves in comparison to the curves by Bohn et al. (2014) are depicted in Fig. S3. 330 Especially for large trees, the differences are significant. Note, however, that the data by Schober (1995) often only include stands with mean DBH of up to 0.75 m (Pinus: 0.43 m, Spruce: 0.44 m, 332 Fagus: 0.54 m, Quercus: 0.70 m, Populus: 0.75 m, Fraxinus: 0.31 m, Betula: 0.27 m, Robinia: 0.41 m). 333 Within this range, the differences between original and updated parameterization are moderate. 334 Equation (S22) is not differentiable everywhere, leading to discontinuities in the maintenance respi-335 ration calculation. Hence, we fitted adjusted biomass curves of form (S23) to the joint equation (S22). 336 Here, we minimized the absolute error between the new curves and B(d) in the interval between the 337 minimal and the maximal DBH of each genus. The resulting curves matched B(d) well. The new 338 parameters are shown in Table S3.

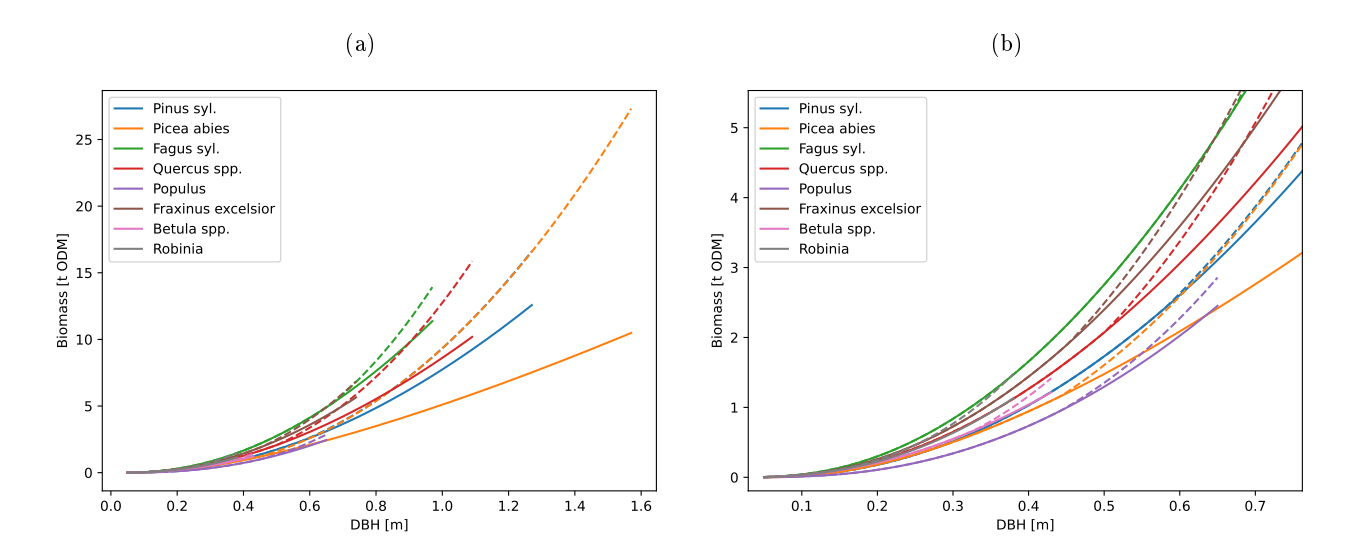


Figure S3: Comparison of the new and old DBH-biomass relationships for the different considered genera. The solid lines depict the relationships as they were in the old parameterization (or $B_0(d)$); the dashed lines show the adjusted relationships (or B(d)). Note that the original biomass equations were fitted to data that only included trees of 0.27 m-0.75 m DBH, where the curves still match relatively well.

	Pinus	Picea	Fagus	Quercus	Populus	Fraxinus	Betula	Robinia
$d_0[\mathrm{m}]$	0.557	1.32	2.45	1.22	1.11	0.998	0.786	1.73
d_1 $[-]$	12.3	10.1	13.8	15.8	13.7	13.4	18.4	9.19

Table S4: Adjusted parameters for the DBH-crown-diameter relationships.

$_{ m 40}$ S5.2.3 DBH-crown-diameter relationships

We refitted the DBH-crown-diameter relationships using the same approach described in section S2.

After an initial investigation, we chose to change the relationship to a simple affine-linear model $D_c(d) = d_0 + d_1 d$, which often also matched the data better. The resulting parameters are provided

in Table S4, and the resulting changes are displayed in Fig. S4.

345 S5.2.4 DBH-LAI relationships

We adjusted the trees' LAI values to approximately match the overall mean value of 3.5 roughly estimated based on LIDAR measurements for the Hohes Holz site (unpublished data). Before the adjustment, the LAI was larger than 5 in the forest area. We adjusted the LAI values for all genera proportionally until we obtained the desired mean value for the forest area. We achieved that by multiplying the LAI values by a factor of about 0.75. Only for Robinia, we kept the original value of 5, as the low maintenance respiration resulting from a small LAI would otherwise have lead to a

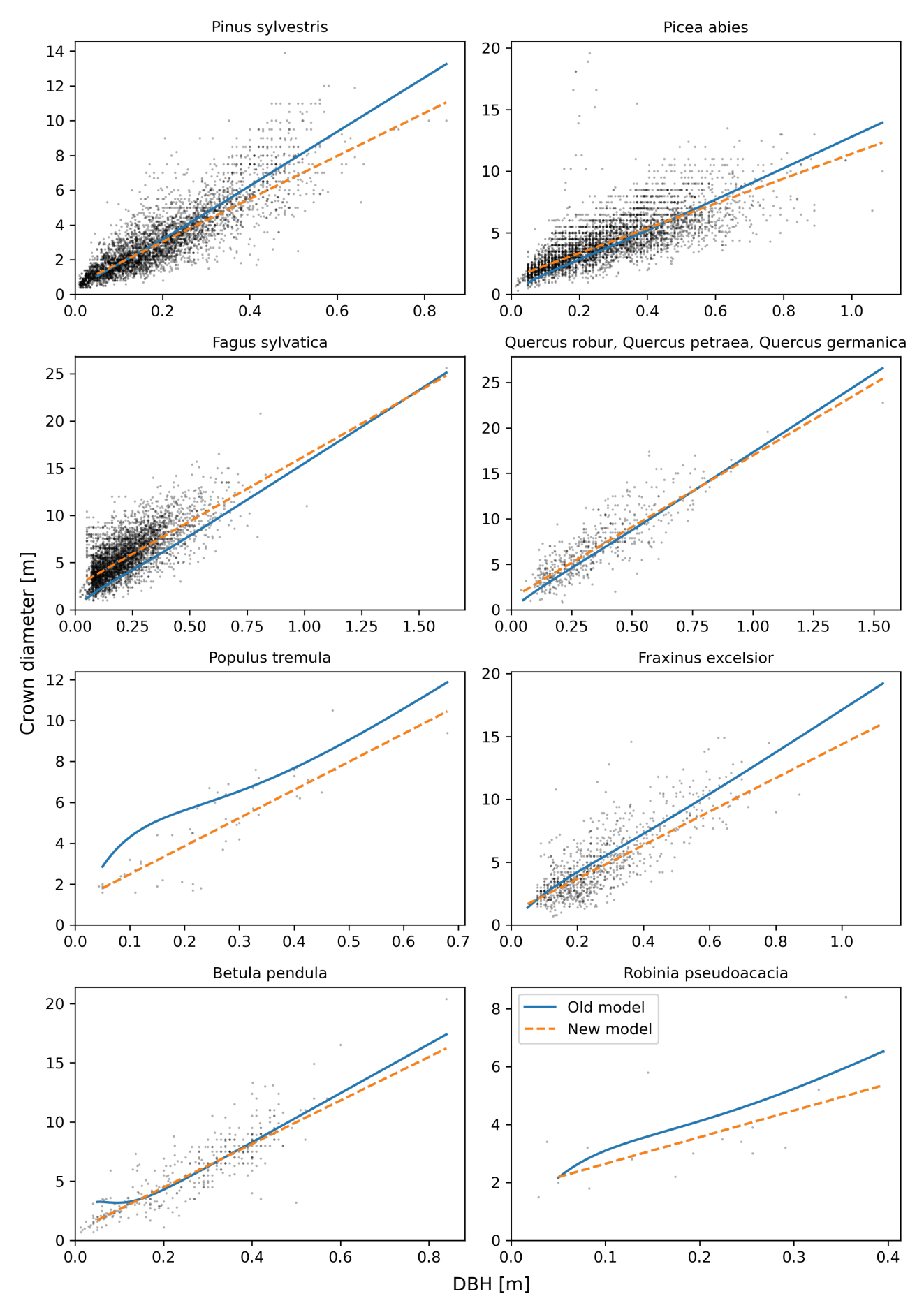


Figure S4: DBH-crown-diameter relationships for the considered species / genera. The black dots display the data from the Tallo database (Jucker et al., 2022); the solid blue curves show the relationships as they were in the old parameterization, whereas the dashed orange lines show the newly fitted curves.

	Pinus	Picea	Fagus	Quercus	Populus	Fraxinus	Betula	Robinia
$ar{d}_0 \; [\mathrm{m}]$	0.05	0.05	0.05	0.05	0.05	0.05	0.05	0.05
$ar{d}_1 \; [ext{m}]$	0.08	0.15	0.1	0.1	0.12	0.07	0.07	0.2
$ar{d}_2 \ [ext{m}]$	0.1	0.25	0.3	0.2	0.25	0.15	0.1	0.2
l ₀ [-]	2.2	1.2	0.596	1.4	1	1.3	1.863	1
l_1 [-]	2.65	3.726	1.49	2.5	2.235	2	2.384	5
l_2 [-]	2.682	5.737	4.545	4.024	3.428	3.726	2.757	5

Table S5: Adjusted parameters for the DBH-LAI relationships.

dominance of this species in simulations of the forest succession.

360

362

linear ansatz for the relationship:

An analysis of the growth of small individuals revealed that they used a high fraction of their GPP
for maintenance respiration (Fig S5). Hence, subtle shading by major trees led to the death of these
plants, hindering the regeneration of the forest. Furthermore, the fraction of GPP used for maintenance
decreased with tree sizes, which disagrees with theoretical results suggesting that the fraction of GPP
used for maintenance should monotonously increase with tree size.

We solved this issue by reducing the LAI for small trees. Due to FORMIND's "inverse" approach
to estimate the maintenance respiration based on reference climate conditions, the maintenance res-

piration is positively related to the LAI. We manually adjusted the DBH-LAI relationship until the

fraction of GPP used for maintenance increased monotonously. To that end, we used a piece-wise

$$L(d) = \begin{cases} l_0 + (d - \bar{d}_0) \frac{l_1 - l_0}{d_1 - d_0} & \text{if } \bar{d}_0 \le d < \bar{d}_1 \\ l_1 + (d - \bar{d}_1) \frac{l_2 - l_1}{\bar{d}_2 - \bar{d}_1} & \text{if } \bar{d}_1 \le d < \bar{d}_2 \\ l_2 & \text{if } \bar{d}_2 \le d, \end{cases}$$
(S24)

where L denotes the LAI, l_0 , l_1 , l_2 are minimal, intermediate, and final LAI value, respectively, \bar{d}_0 is the initial DBH of seedlings, and \bar{d}_1 and \bar{d}_2 are the DBH values where the intermediate and the final LAI are attained, respectively. The changes affected small trees only and did not decrease the overall LAI of the Hohes Holz forest significantly. The chosen parameters are displayed in Table S5; the resulting LAI and respiration curves are depicted in Fig. S5.

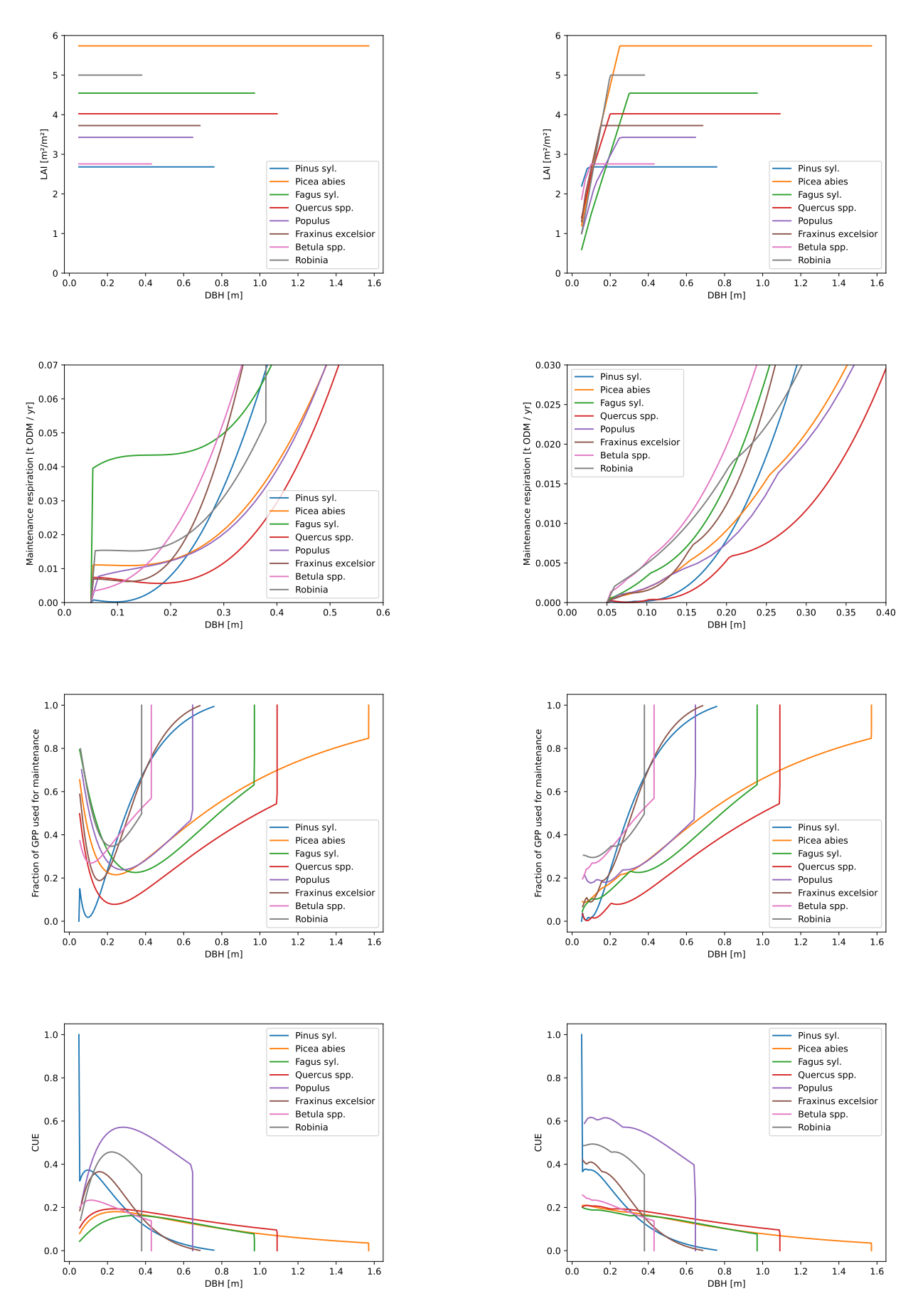


Figure S5: Impact of the LAI on carbon usage. All figures were created with the same parameterization except that the LAI was kept constant in the left figures, whereas it was adjusted in the right figures. If the LAI is kept constant, the maintenance respiration of small trees is high, leading to an initial decrease in the fraction of the GPP required for maintenance.

368 S5.2.5 Maximal height for Robinia

We changed the maximal height for Robinia from 27.3 m to 34 m. Without this adjustment, the maximal height would have corresponded to a relatively small maximal diameter at breast height (DBH) according to the new height-stem-diameter relationship. As FORMIND uses the DBH as central measure fore tree size internally, the small maximal diameter would have limited tree growth very early. The new height maximum was determined based on the Tallo database (Jucker et al., 2022).

374 S5.2.6 Light extinction coefficient

We reduced the light extinction coefficient from 0.7 to 0.5. This parameter change increases the potential forest density and is in line with common radiative transfer model parameterizations (Yang et al., 2017) and the parameterization by Fischer et al. (2024).

378 S5.2.7 Soil and weather parameters

- We adjusted the soil and weather parameters based on the conditions found at the Hohes Holz site.
- The initial soil water content was set to a value of 21% (v/v) so that the soil water content does not change significantly over time (i.e., directly hits its equilibrium) at the Hohes Holz site.
- The mean rainfall duration for rainy days was reduced from $24 \frac{h}{day}$ to a value of $6 \frac{h}{day}$.
- The soil rooting depth was reduced from 20 m to 2 m, which reflects the soil conditions at the

 Hohes Holz site.
- The permanent wilting point was adjusted from 20.8% to 13.3% according to Maidment (1993) p. 5.14 (silt loam soil; water retained at $-1500\,\mathrm{kPa}$).
- The field capacity was changed from 36.6% to 33% according to Maidment (1993) p. 5.14 (silt loam soil; water retained at -33 kPa).
- The soil porosity was increased from 46.3% to 50.1% according to field measurements at the

 Hohes Holz site. An identical value is shown in Maidment (1993) p. 5.14 (silt loam soil).
- The fully saturated conductivity was adjusted from a value of $3.66 \cdot 10^{-6} \frac{\text{m}}{\text{s}}$ to $6.944 \cdot 10^{-7} \frac{\text{m}}{\text{s}}$ according to the value displayed in Fig. 5.3.3 on p. 5.16 in Maidment (1993); value estimated for 7.6% sand, 14.9% clay, and 77.5% silt (soil composition of Hohes Holz).
- The pore size distribution index was set from 0.252 to 0.234 according to Maidment (1993) p. 5.14 (silt loam soil).

• The residual soil water content was reduced from 2.7 to 1.5 according to Maidment (1993) p.
5.14 (silt loam soil).

S5.2.8 Climatic reference conditions

398

The climatic reference conditions denote the growth conditions of an unshaded tree within a forest with typical climate. The reference conditions are needed to compute the maintenance respiration of trees by comparing the GPP of a tree under reference conditions with the observed growth of such a tree. The carbon difference between GPP and observed wood production is assumed to be used for respiration and other losses.

For performance reasons, the GPP of the tree under reference conditions is computed under "mean" 404 conditions for an entire year rather than on a daily resolution. Since several model processes are non-405 linear, the reference conditions (e.g. reference irradiation) are not simply given by a yearly mean (e.g. 406 mean yearly irradiance) but need to be determined via a more intricate approach. Here, the goal is to 407 achieve that a reference tree simulated with yearly time step has approximately the same GPP, NPP, and respiration as a tree simulated under the same conditions but on a daily resolution. This goal also drove our general approach: we considered two trees x_0 and x_1 simulated with a yearly and a daily 410 time step, respectively, and adjusted the property in question (e.g. the irradiance) of x_0 until its GPP 411 and NPP matched the one of tree x_1 . 412

Below, we used a "mean" daily climate for the reference conditions. That is, we averaged the climate from the years 2000-2017 at a site (longitude 11.5, latitude 51.8) close to the Hohes Holz area (longitude 11.22, latitude 52.09) for each day of the year.

S5.2.8.1 Reference vegetation period length We retrieved the length of the vegetation period directly by simulating the forest under reference conditions for one year with a daily step. The length of the vegetation period can be directly used in the simplified model version with yearly time step. We obtained a value of 0.57 yr for the mean vegetation period length.

S5.2.8.2 Reference irradiance We considered a simple and an advanced model to estimate the reference irradiation, where the simple model used a constant irradiance and day length, corresponding to the respective averages in the vegetation period, whereas the advanced model considered day length and irradiance on a daily basis. For each genus, we considered an individual with a DBH half as big as its maximal DBH and adjusted the mean incoming irradiance of the simple model until the GPP of the trees in the simple and the advanced model matched. Since the GPP scales linearly with day length, only one of mean irradiance and mean day length are identifiable, and we could set the mean

	Pinus	Picea	Fagus	Quercus	Populus	Fraxinus	Betula	Robinia
Ref. irradiance $\left[\frac{\mu \text{Mol photon}}{\text{m}^2 \cdot \text{s}}\right]$	553.760	552.686	893.750	833.594	842.188	893.750	833.594	842.188
Ref. GPP reduction $[-]$	0.798	0.788	0.802	0.806	0.853	0.844	0.800	0.865

Table S6: Adjusted parameters for reference climatic conditions.

day length to a value of 12 h in the simple model without loss of accuracy.

Since the light response curves are genus-dependent, we obtained a different reference irradiance for each genus. In particular, the reference irradiance was lower for evergreen trees than for deciduous trees, as the latter do not grow in winter. The updated reference irradiance values can be found in Tab. S6.

432 **S5.2.8.3 Reference GPP reduction** The reference GPP reduction specifies by how much the GPP of a tree under reference conditions is reduced by environmental factors. As water competition depends on all trees in a patch, we needed to consider reference trees with "usual" competition. We considered all $20 \,\mathrm{m} \times 20 \,\mathrm{m}$ patches with a biomass of at least $15 \,\mathrm{t} \,\mathrm{ODM} = 375 \,\frac{\mathrm{t} \,\mathrm{ODM}}{\mathrm{ha}}$ in the inventory and searched for each genus an unshaded tree, which we then used as reference tree. For this tree, we determined the GPP with and without reduction by water competition and temperature effects. The desired reduction factor was the quotient of these two numbers.

If a genus was not present in the inventory, we identified the largest unshaded tree in the inventory with a DBH below the genus' maximal DBH and changed the selected tree's genus to the genus we wanted to consider. Then we used the selected tree as reference tree. The reference GPP reduction factors are displayed in Tab. S6.

443 S5.2.9 Respiratory losses

To determine the extent of trees' carbon losses not required for maintenance, we applied the approach proposed by Fischer et al. (2024). Based on the light climate, we determined for each tree in the forest the maximal maintenance respiration that the tree could satisfy with his GPP at its location, assuming that

$$GPP \ge maintenance respiration.$$
 (S25)

This formula should hold for most trees in general, but due to model simplifications (e.g., discretization of space), some trees observed in the inventory may not satisfy this condition for GPP and maintenance respiration computed with FORMIND.

In FORMIND, the carbon balance of each tree is closed, i.e.,

$$GPP = NPP + maintenance respiration + other losses,$$
 (S26)

where NPP and the loss term are proportional:

other losses =
$$\frac{\gamma}{1-\gamma}$$
NPP,

so that we can write

451

$$NPP = (1 - \gamma) (GPP - maintenance respiration), (S27)$$

or equivalently

455

maintenance respiration =
$$GPP - \frac{NPP}{1-\gamma}$$
, (S28)

where γ is the loss factor. As equation (S28) holds in particular for trees under reference conditions, whose NPP is known, the maintenance respiration is directly related to γ , and a change in γ impacts 456 how many trees in the inventory satisfy inequality (S25). We identified the value of γ , where (S25) 457 holds for 90% of the trees at Hohes Holz. If we considered each genus independently, the following 458 values for the loss fraction would be required: Pinus: 0.63, Picea: 0.72, Fagus: 0.77, Quercus: 0.71, Betula: 0.74. If we considered all individuals simultaneously, a value of 0.77 would be necessary. 460 We used these growth loss factors γ as basis for the parameterization but adjusted them based 461 on follow-up considerations. For Pinus, the GPP under reference conditions was not high enough to 462 support 63% losses for trees of certain sizes. That is, the maintenance respiration was typically small 463 enough to satisfy inequality (S25), but for small trees, we observed that $(1-\gamma)$ GPP < NPP under reference conditions. Therefore, we reduced the loss value to $\gamma = 0.62$. For Picea, Fagus, and for 465 Quercus, we increased the loss values so as to allow for a sufficient density and diversity of forests in 466 succession runs. For Betula, we decreased the loss value to prevent it from becoming the dominant 467 species in succession runs. 468 We chose loss values for the genera not present in the Hohes Holz area by matching the other genera's fraction of GPP used for maintenance respiration (Fig. S5). However, Populus and Robinia had a very high carbon use efficiency, making them extremely competitive in simulations. Therefore, 471 we set their growth loss fractions to smaller values (0.25 and 0.3, respectively), which match the values 472 from earlier FORMIND parameterizations. This manual fine tuning was necessary due to a lack of data needed for a more rigorous approach. The final chosen values for γ are displayed in Table S7.

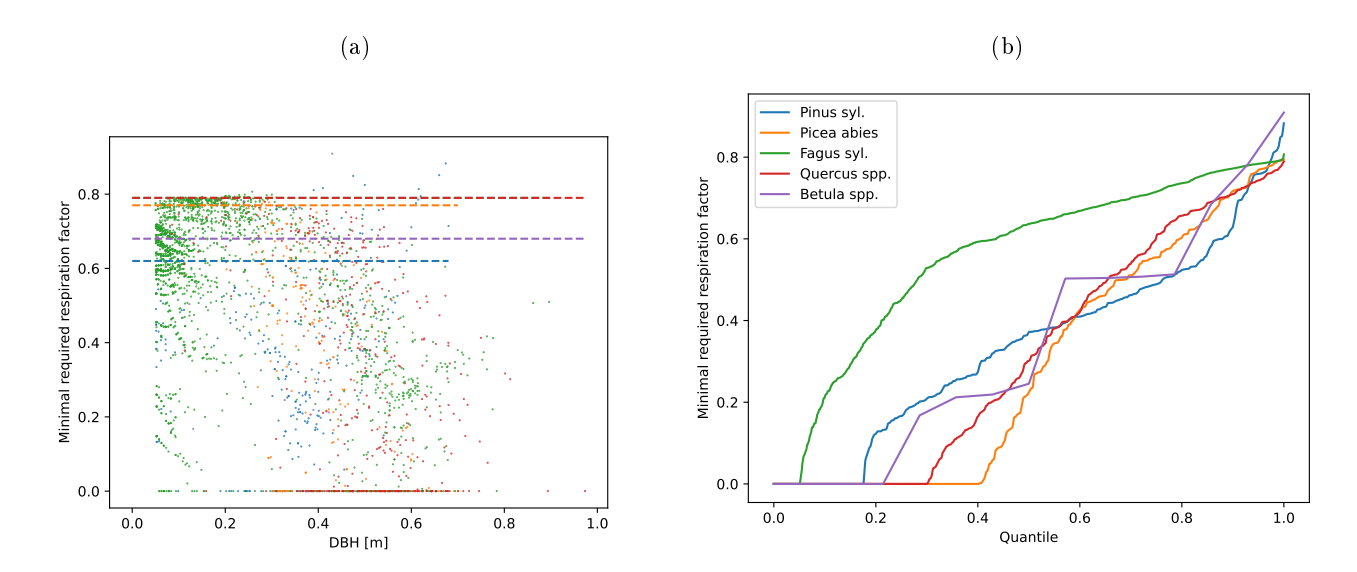


Figure S6: (a) Minimal required loss (here: "respiration") factor γ required to satisfy inequality (S25) for each tree in the inventory. Each dot corresponds to a tree; the dashed lines correspond to the values of γ used in the parameterization. (b) Minimal respiration factor γ required to satisfy inequality (S25) for the given quantiles (fractions) of each genus' individuals.

	Pinus	Picea	Fagus	Quercus	Populus	Fraxinus	Betula	Robinia
Respiration / loss factors [-]	0.62	0.77	0.79	0.79	0.25	0.55	0.68	0.3

Table S7: Adjusted respiration / loss factors.

	Pinus	Picea	Fagus	Quercus	Populus	Fraxinus	Betula	Robinia
Mortality scaling $a \left[\frac{1}{yr} \right]$	0.0027	0.0045	0.0062	0.0046	0.0119	0.0020	0.0129	0.0084
Mortality exponent b $[-]$	-1.271	-0.953	-0.761	-0.950	-0.894	-1.505	-0.210	-0.373

Table S8: Adjusted parameters for the DBH-dependent mortality function $\mathbb{P}(\text{death}) = a \cdot \text{DBH}^b$.

475 S5.2.10 Mortality

We enabled the defoliation mechanism (first introduced by Fischer et al., 2024) as a consistent way
to account for trees whose respiratory needs exceed their gross primary productivity (GPP). As both
respiration and GPP depend on weather conditions and water supply, this mechanism also allows
modelling the impact of climatic conditions (e.g. drought) on mortality. We disabled the earlier
approach for handling trees whose respiration exceed their GPP, which had assigned such trees an
increased stochastic mortality rate.

As trees could die due to loss of leafs after the aforementioned update, we reduced the DBHdependent stochastic background mortality probabilities for all species by factor 0.705 in turn. This
factor was chosen so that the forest biomass obtained in long succession runs matched the biomass in
the inventory. The updated parameter values can be found in Table S8.

486 S5.2.11 Regeneration

The original parameterization by Bohn et al. (2014) did not consider regeneration. As no data for parameterizing ingrowth were available to us, we assumed that regeneration is not limited by the number of seeds but rather the available light. Hence, we set the number of in-growing saplings to a large number $(100 \frac{1}{\text{ha}\cdot\text{yr}})$.

491 S5.3 Analysis of the new parameterization

With the adjusted parameterization, we obtained the following main characteristics of the Hohes Holz forest, initialized based on the inventory:

494 **Biomass:** $326.79 \frac{\text{t ODM}}{\text{ha}}$

Stem count: $214.61 \frac{1}{ha}$

Basal area: $27.49 \frac{\text{m}^2}{\text{ha}}$

497 **LAI**: 3.5

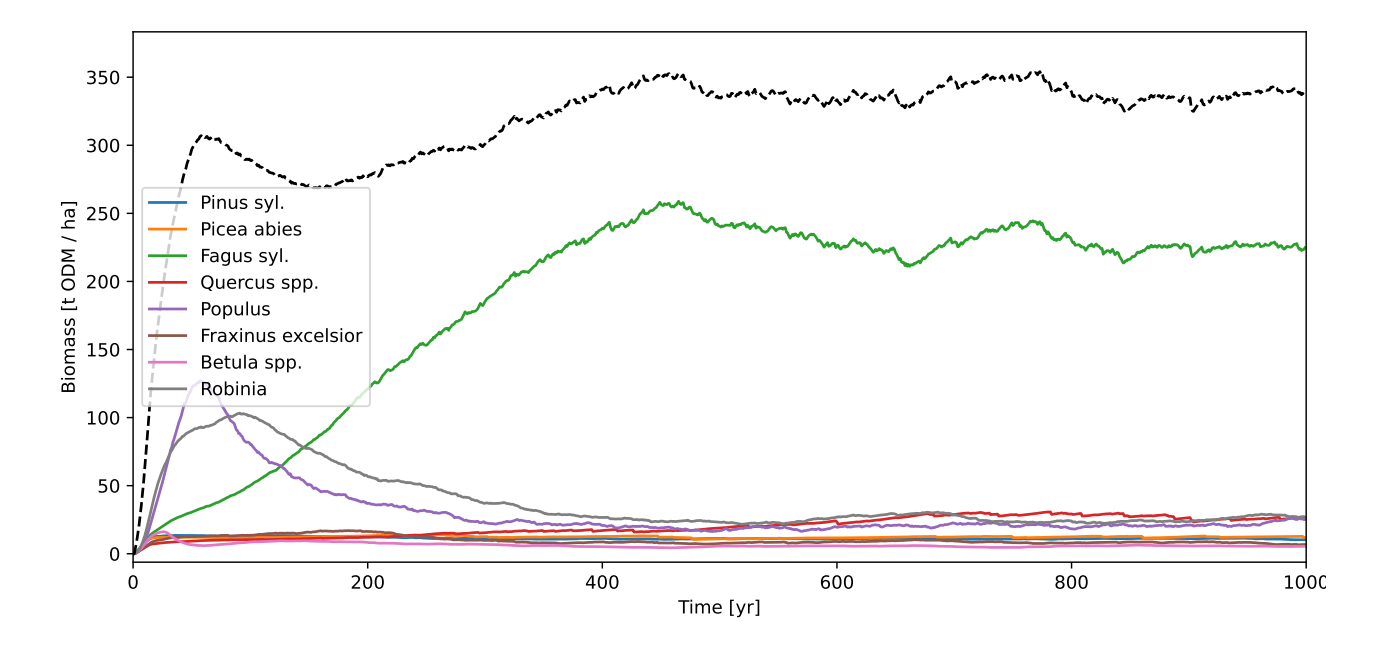


Figure S7: Succession of 8 ha forest under the climatic conditions of Hohes Holz (2000-2017).

```
GPP: 34.46 \frac{\text{tODM}}{\text{ha·yr}} (2015: 32.9 \frac{\text{tODM}}{\text{ha·yr}} c.f. measured value of 38 \pm 3 \frac{\text{tODM}}{\text{ha·yr}}; Pohl et al., 2023)

NPP: 4.17 \frac{\text{tODM}}{\text{ha·yr}} (2015: 3.70 \frac{\text{tODM}}{\text{ha·yr}} c.f. measured NEP value of 7 \pm 0.7 \frac{\text{tODM}}{\text{ha·yr}}; Pohl et al., 2023)

Respiration: 34.29 \frac{\text{tODM}}{\text{ha·yr}} (2015: 29.19 \frac{\text{tODM}}{\text{ha·yr}} c.f. measured ecosystem respiration value of 31 \pm 3.6 \frac{\text{tODM}}{\text{ha·yr}}; Pohl et al., 2023)
```

The reference values by Pohl et al. (2023) were measured via an on-site Eddy-flux tower.

Most of the main forest characteristics matched field estimates in their order of magnitude. Only
the NPP was lower than expected, since the measured NEP value, which is a lower bound for NPP, is
almost twice as big as the modelled NPP.

If the model is run from bare ground, FORMIND predicts the emergence of a beech-dominated forest at the Hohes Holz site (see Fig. S7). In the first 200 years, fast-growing genera (Populus and Robinia)
dominate, but Betula always remains at a low density. After 400 years, the forest composition remains
roughly constant. Conifers play a minor role; Quercus becomes the second-most abundant genus.

510 References

Akaike, H. (1974). A new look at the statistical model identification. *IEEE Transactions on Automatic*Control, 19(6):716–723.

Bohn, F. J., Frank, K., and Huth, A. (2014). Of climate and its resulting tree growth: Simulating the productivity of temperate forests. *Ecological Modelling*, 278:9–17.

- Bohn, F. J. and Huth, A. (2017). The importance of forest structure to biodiversity-productivity relationships. *Royal Society Open Science*, 4(1):160521.
- Fischer, S. M., Wang, X., and Huth, A. (2024). Distinguishing mature and immature trees allows estimating forest carbon uptake from stand structure. *Biogeosciences*, 21(14):3305–3319.
- Henniger, H., Bohn, F. J., Schmidt, K., and Huth, A. (2023a). A new approach combining a multilayer
- radiative transfer model with an individual-based forest model: Application to boreal forests in
- Finland. Remote Sensing, 15(12):3078.
- Henniger, H., Huth, A., Frank, K., and Bohn, F. J. (2023b). Creating virtual forests around the globe
- and analysing their state space. Ecological Modelling, 483:110404.
- Holtmann, A., Huth, A., Pohl, F., Rebmann, C., and Fischer, R. (2021). Carbon Sequestration in
- Mixed Deciduous Forests: The Influence of Tree Size and Species Composition Derived from Model
- Experiments. Forests, 12(6):726.
- Jucker, T., Fischer, F. J., Chave, J., Coomes, D. A., Caspersen, J., Ali, A., Loubota Panzou, G. J.,
- Feldpausch, T. R., Falster, D., Usoltsev, V. A., Adu-Bredu, S., Alves, L. F., Aminpour, M., Angoboy,
- I. B., Anten, N. P. R., Antin, C., Askari, Y., Muñoz, R., Ayyappan, N., Balvanera, P., Banin, L.,
- Barbier, N., Battles, J. J., Beeckman, H., Bocko, Y. E., Bond-Lamberty, B., Bongers, F., Bowers,
- 531 S., Brade, T., van Breugel, M., Chantrain, A., Chaudhary, R., Dai, J., Dalponte, M., Dimobe, K.,
- Domec, J.-C., Doucet, J.-L., Duursma, R. A., Enríquez, M., van Ewijk, K. Y., Farfán-Rios, W.,
- Fayolle, A., Forni, E., Forrester, D. I., Gilani, H., Godlee, J. L., Gourlet-Fleury, S., Haeni, M., Hall,
- J. S., He, J.-K., Hemp, A., Hernández-Stefanoni, J. L., Higgins, S. I., Holdaway, R. J., Hussain, K.,
- Hutley, L. B., Ichie, T., Iida, Y., Jiang, H.-s., Joshi, P. R., Kaboli, H., Larsary, M. K., Kenzo, T.,
- Kloeppel, B. D., Kohyama, T., Kunwar, S., Kuyah, S., Kvasnica, J., Lin, S., Lines, E. R., Liu, H.,
- Lorimer, C., Loumeto, J.-J., Malhi, Y., Marshall, P. L., Mattsson, E., Matula, R., Meave, J. A.,
- Mensah, S., Mi, X., Momo, S., Moncrieff, G. R., Mora, F., Nissanka, S. P., O'Hara, K. L., Pearce, S.,
- Pelissier, R., Peri, P. L., Ploton, P., Poorter, L., Pour, M. J., Pourbabaei, H., Dupuy-Rada, J. M.,
- Ribeiro, S. C., Ryan, C., Sanaei, A., Sanger, J., Schlund, M., Sellan, G., Shenkin, A., Sonké, B.,
- Sterck, F. J., Svátek, M., Takagi, K., Trugman, A. T., Ullah, F., Vadeboncoeur, M. A., Valipour,
- A., Vanderwel, M. C., Vovides, A. G., Wang, W., Wang, L.-Q., Wirth, C., Woods, M., Xiang, W.,
- Ximenes, F. d. A., Xu, Y., Yamada, T., and Zavala, M. A. (2022). Tallo: A global tree allometry
- and crown architecture database. Global Change Biology, 28(17):5254-5268.
- Kattge, J., Díaz, S., Lavorel, S., Prentice, I. C., Leadley, P., Bönisch, G., Garnier, E., Westoby, M.,

- Reich, P. B., Wright, I. J., Cornelissen, J. H. C., Violle, C., Harrison, S. P., Van Bodegom, P. M.,
- Reichstein, M., Enquist, B. J., Soudzilovskaia, N. A., Ackerly, D. D., Anand, M., Atkin, O., Bahn,
- M., Baker, T. R., Baldocchi, D., Bekker, R., Blanco, C. C., Blonder, B., Bond, W. J., Bradstock,
- R., Bunker, D. E., Casanoves, F., Cavender-Bares, J., Chambers, J. Q., Chapin Iii, F. S., Chave,
- J., Coomes, D., Cornwell, W. K., Craine, J. M., Dobrin, B. H., Duarte, L., Durka, W., Elser, J.,
- Esser, G., Estiarte, M., Fagan, W. F., Fang, J., Fernández-Méndez, F., Fidelis, A., Finegan, B.,
- Flores, O., Ford, H., Frank, D., Freschet, G. T., Fyllas, N. M., Gallagher, R. V., Green, W. A.,
- Gutierrez, A. G., Hickler, T., Higgins, S. I., Hodgson, J. G., Jalili, A., Jansen, S., Joly, C. A.,
- Kerkhoff, A. J., Kirkup, D., Kitajima, K., Kleyer, M., Klotz, S., Knops, J. M. H., Kramer, K.,
- Kühn, I., Kurokawa, H., Laughlin, D., Lee, T. D., Leishman, M., Lens, F., Lenz, T., Lewis, S. L.,
- Lloyd, J., Llusià, J., Louault, F., Ma, S., Mahecha, M. D., Manning, P., Massad, T., Medlyn, B. E.,
- Messier, J., Moles, A. T., Müller, S. C., Nadrowski, K., Naeem, S., Niinemets, Ü., Nöllert, S., Nüske,
- A., Ogaya, R., Oleksyn, J., Onipchenko, V. G., Onoda, Y., Ordoñez, J., Overbeck, G., Ozinga,
- W. A., Patiño, S., Paula, S., Pausas, J. G., Peñuelas, J., Phillips, O. L., Pillar, V., Poorter, H.,
- Poorter, L., Poschlod, P., Prinzing, A., Proulx, R., Rammig, A., Reinsch, S., Reu, B., Sack, L.,
- Salgado-Negret, B., Sardans, J., Shiodera, S., Shipley, B., Siefert, A., Sosinski, E., Soussana, J.-F.,
- 562 Swaine, E., Swenson, N., Thompson, K., Thornton, P., Waldram, M., Weiher, E., White, M., White,
- S., Wright, S. J., Yguel, B., Zaehle, S., Zanne, A. E., and Wirth, C. (2011). TRY a global database
- of plant traits. Global Change Biology, 17(9):2905–2935.
- Lukeš, P., Stenberg, P., Rautiainen, M., Mõttus, M., and Vanhatalo, K. M. (2013). Optical properties
- of leaves and needles for boreal tree species in Europe. Remote Sensing Letters, 4(7):667-676.
- Maidment, D. R., editor (1993). Handbook of Hydrology. McGraw-Hill, New York.
- Medlyn, B. E., Badeck, F. W., De Pury, D. G. G., Barton, C. V. M., Broadmeadow, M., Ceulemans,
- R., De Angelis, P., Forstreuter, M., Jach, M. E., Kellomäki, S., Laitat, E., Marek, M., Philippot,
- 570 S., Rey, A., Strassemeyer, J., Laitinen, K., Liozon, R., Portier, B., Roberntz, P., Wang, K., and
- Jstbid, P. G. (1999). Effects of elevated [CO₂] on photosynthesis in European forest species: A
- meta-analysis of model parameters. Plant, Cell & Environment, 22(12):1475–1495.
- Pohl, F., Werban, U., Kumar, R., Hildebrandt, A., and Rebmann, C. (2023). Observational evidence
- of legacy effects of the 2018 drought on a mixed deciduous forest in Germany. Scientific Reports,
- 575 13(1):10863.
- Schober, R. (1995). Ertragstafeln wichtiger Baumarten bei verschiedener Durchforstung. Sauerländer,
- Frankfurt am Main, 4. aufl edition.

- 578 Verhoef, W. (1998). Theory of Radiative Transfer Models Applied in Optical Remote Sensing of Vege-
- tation Canopies. PhD thesis, Wageningen University and Research.
- ⁵⁸⁰ Wand, M. P. and Jones, M. C. (1995). Kernel Smoothing. Number 60 in Monographs on Statistics
- and Applied Probability. Chapman & Hall, London; New York, 1st ed edition.
- Yang, P., Verhoef, W., and van der Tol, C. (2017). The mSCOPE model: A simple adaptation to the
- SCOPE model to describe reflectance, fluorescence and photosynthesis of vertically heterogeneous
- canopies. Remote Sensing of Environment, 201:1-11.